An Improved Adaptive Selected Harmonic Elimination Algorithm for Current Measurement Error Correction of PMSMs

Kai Zhang, *Graduate Student Member, IEEE*, Mingdi Fan, *Senior Member, IEEE*, Yong Yang, *Senior Member, IEEE*, Zhongkui Zhu, Cristian Garcia, *Member, IEEE*, and Jose Rodriguez, *Life Fellow, IEEE*

***Abstract*—Measurement errors are inevitable in the current sensors, which cause speed ripple including one and twice the stator electrical frequency. For the undesired harmonics, the adaptive selected harmonic elimination (ASHE) algorithm outputs the sum of the sinusoidal signals multiplied by the adaptive weights. In order to solve the current measurement error (CME) issue, this article adopts the ASHE algorithm. According to the deterministic functional relationship of the surface-mounted permanent magnet synchronous motor (SPMSM), the adopted algorithm extracts the harmonics of the steady state speed error, and outputs the *q*-axis current compensation. However, there is no explicit connection between speed and *d*-axis current, so their relationship is uncertain. The remaining *d*-axis CMEs result in poor current performance. Therefore, this article proposes an improved ASHE algorithm, which compensates the *dq*-axis CMEs simultaneously depending on their mutual deterministic connection. The proposed method does not need motor parameters, additional sensors, or complex calculation process. Finally, the effectiveness of the method is verified by the SPMSM platform. Experimental results also show that the proposed method reduces speed ripple and suppresses the negative effects of CMEs.**

***Index Terms*—Adaptive selected harmonic elimination (ASHE), current measurement errors (CMEs), permanent magnet synchronous motor (PMSM), vector control (VC).**

Manuscript received March 22, 2021; accepted April 27, 2021. Date of publication May 3, 2021; date of current version July 30, 2021. This work was supported in part by the National Natural Science Foundation of China under Grants 51907137, 51977136, and 51707127, in part by the Jiangsu Planned Projects for Postdoctoral Research Funds under Grant 2020Z444, in part by the China Postdoctoral Science Foundation under Grant 2020M681693, in part by the Agencia Nacional de Investigacion y Desarrollo (ANID)/Fondo Nacional de Desarrollo Cientifico y Tecnologico (FONDECYT) through Initiation Research Project under Grant 11180235, and in part by the ANID under Projects FB0008, ACT192013, and 1210208. Recommended for publication by Associate Editor R. Kennel. *(Corresponding author: Mingdi Fan.)*

Kai Zhang, Mingdi Fan, Yong Yang, and Zhongkui Zhu are with the School of Rail Transportation, Soochow University, Suzhou 215131, China (e-mail: kzhang10@stu.suda.edu.cn; mdfan@suda.edu.cn; yangy1981@suda.edu.cn; zhuzhongkui@suda.edu.cn).

Cristian Garcia is with the Faculty of Engineering, Universidad de Talca, Curico 3340000, Chile (e-mail: cristian.garcia@utalca.cl).

Jose Rodriguez is with the Department of Engineering Science, Faculty of Engineering, Universidad Andres Bello, Santiago 8370146, Chile (e-mail: jose.rodriguez@unab.cl).

Color versions of one or more figures in this article are available at https://doi.org/10.1109/TPEL.2021.3076993.

Digital Object Identifier 10.1109/TPEL.2021.3076993

I. Introduction

With the advanced power electronic technology, ac machines have dominated the traction machine market [1]. Among various ac machines, permanent magnet synchronous motor (PMSM) has many features, such as operation over a wide torque speed range, high power, density, etc. It receives abundant attention and is widely applied in industrial fields and electrified transportation [2]–[4]. Aiming to attain fine servo performance, relying on sensors to sample electrical signals, modern control technologies perform closed-loop control. Among these control technologies, vector control (VC) is very common. In detail, traditional VC requires two current sensors and an encoder [5], [6]. For the motor drives, current and speed feedback are essential.

Current feedback is generally phase current, which is the voltage signal output by the sensor. It is processed by an analog-digital converter (ADC) through matching circuits and noise filter circuits. Due to the circuit nonlinearity, the operating environment, especially temperature variation, even if the system is well constructed, current measurement errors (CMEs) are still inevitable [7]. CMEs mainly include offset error and scaling error, which generate torque pulsation, subsequently yielding speed ripple of single and double fundamental frequencies [8]–[10]. Therefore, these CMEs need to be restricted or compensated. The simplest method is to update the error correction when the motor is down. However, except that the offset error may change due to thermal drift, and this method not only interferes with normal operation but also fail to handle the scale error. Hence, different online compensation methods are proposed.

For online compensation of CMEs, some methods use additional sensors. In [8], the dc-bus current is utilized for mutual calibration of sensors. By means of one voltage sensor, [9] and [10] estimate the stator currents and design controllers to eliminate CMEs. Via the torque transducer, [11] obtains the steady state torque error, and iteratively learns to compensate the current references. There are other methods compensating current references, such as filtering the difference between the predicted and measured currents [12] and exploiting the transfer function of torque disturbance to speed error [13]. In [14],

repetitive control is performed depending on the stored voltage errors. Based on the disturbance observer, [15] designs a composite voltage compensator and [16] directly confirms the offset and gains by the positive sequence component estimator. Moreover, [17] analyzes that the integrator output of the *d*-axis proportional integral (PI) current regulator is constant, subtracts offset errors, and rescales the gains. By injecting high-frequency voltage, [18] acquires the positive and negative sequence currents to scale the gains. In [19], with isolation and decoupling matrix, the regulator estimates the gains by minimizing the current differential gains. Although above methods compensate CMEs, they may use additional sensors, rely on motor parameters, or have a complicated calculation process.

In addition, there is a classic adaptive notch canceller that eliminates sinusoidal interference in digital signal processing [20]. For power electronic applications, [21] proposes an adaptive select harmonic elimination (ASHE) algorithm, which only requires knowledge of the harmonic frequency. The general framework, theories and methods of harmonic component elimination is described in [22]. In terms of specific applications, [23] applies adaptive filters to shunt active power filters to improve the transient response time of harmonic detection. Besides, the ASHE algorithm is introduced to a three-level T-type inverter to eliminate the 5th-31st harmonics [24]. Regarding motor drives, [25] uses the same structure to diminish the harmonics in the rotor estimation error of sensorless control. Based on the least mean square (LMS) algorithm, [26] compensates the voltage references and suppresses deadtime current distortion in VC. In general, the sole function of ASHE algorithm is to eliminate undesirable higher-order harmonics from the selected variable.

Correspondingly, CMEs cause torque pulsation, thereby resulting in speed ripple with single and double fundamental frequencies. This article adopts the ASHE algorithm to reduce speed ripple of the surface-mounted PMSM. Through the deterministic functional relationship, speed ripple originates from *q*-axis CMEs. The adopted ASHE algorithm outputs the *q*-axis current compensation, which reduces speed ripple. However, the *d*-axis CMEs are not compensated, resulting in poor current performance. Furthermore, the relationship between speed and *d*-axis current is uncertain. In order to completely suppress the negative impact of CMEs, this article improves the ASHE algorithm. Considering that the *dq*-axis CMEs are the weighted sums of sinusoidal signals, their mutual connection is deterministic. Then, the *d*-axis current compensation can be obtained by adaptive weights of the ASHE algorithm. The *dq*-axis CMEs are compensated simultaneously and respectively. Without motor parameters, additional sensors or complex calculation processes, the proposed method reduces speed ripple and suppresses the negative effects of CMEs.

This article is organized as follows. In Section II, the PMSM model, CMEs and related limits of traditional method are illustrated. In Section III, the principle and implementation of the ASHE algorithm, further improvement, and application are presented. The experimental results are shown in Section IV. Finally, Section V concludes the article.

II. Effects of Motor CMEs

A. Mathematical Model of PMSMs

Aiming at the CMEs of various motors, this article takes the PMSM as an example. In the *dq*-synchronous reference frame, the mathematical model of PMSM is as follows:

$$\begin{aligned}\frac{di_d}{dt} &= -\frac{R_s}{L_d}i_d + \frac{L_q\omega_e}{L_d}i_q + \frac{1}{L_d}u_d \\ \frac{di_q}{dt} &= -\frac{L_d\omega_e}{L_q}i_d - \frac{R_s}{L_q}i_q + \frac{1}{L_q}u_q - \frac{\psi_{PM}\omega_e}{L_q} \\ J\frac{d\omega_m}{dt} &= T_e - T_L \end{aligned} \tag{1}$$

where u_d and u_q are the stator *dq*-axis voltage, i_d and i_q are the stator *dq*-axis current, L_d and L_q are *dq*-axis inductance, ψ_{PM} is the permanent magnet flux linkage, R_s is the stator winding resistance, ω_e is the electrical angular speed, $\omega_e = p\omega_m$, p represents the number of pole pairs, and ω_m is the mechanical angular speed. Finally, J, T_e, and T_L are the rotational inertia, the electrical torque, and load torque, respectively.

As for the traditional VC with $i_d^* = 0$ (i.e., maximum torque per ampere in torque control), or the surface-mounted permanent magnet synchronous motor (SPMSM), whose stator inductance $L_s = L_d = L_q$, the electromagnetic torque can be described as

$$\begin{aligned} T_e &= 1.5p\left(\psi_{\mathrm{PM}}i_q + (L_d - L_q)\, i_d i_q\right) \\ &= 1.5p\psi_{\mathrm{PM}}i_q = k_T i_q. \end{aligned} \tag{2}$$

Substituting (2) into the motor motion equation in (1), the relationship between speed and *q*-axis current can be obtained

$$J\frac{d\omega_m}{dt} = k_T i_q - T_L. \tag{3}$$

Thus, the relationship between current and speed is established through the connection of torque, current, and speed.

B. Analysis of CMEs

The stator current is first converted into a voltage signal by the sensor, and then discretized into a digital value by a low-pass filter and ADC. The factors that may cause CMEs include the sensor itself, signal processing circuits, differences between sampling circuits, discrete errors in ADC, and other factors such as thermal drift, magnetic field interference, etc. [20]. Therefore, CMEs inevitably exist under these factors.

Usually, the classic three-phase three-wire circuit topology uses two sensors to measure any two-phase currents. This article takes phases *a* and *b* as an example, and phase *c* current is obtained by Kirchhoff's current law. Then, the measured values of the three-phase currents are expressed as

$$\begin{cases} i_{a\_\mathrm{mea}} = k_a i_{a\_\mathrm{act}} + \Delta i_{a\_\mathrm{offset}} \\ i_{b\_\mathrm{mea}} = k_b i_{b\_\mathrm{act}} + \Delta i_{b\_\mathrm{offset}} \\ i_{c\_\mathrm{mea}} = -i_{a\_\mathrm{mea}} - i_{b\_\mathrm{mea}} \end{cases} \tag{4}$$

where i_{x_mea} and i_{x_act}, $x = a, b, c$, are the measured and actual values of three phase currents, and such as phase a, k_a, and $\Delta i_{a\_\mathrm{offset}}$ are the offset error and scaling error, respectively.

After Clark and Park transformation, the *dq*-synchronous rotating currents are obtained

$$\begin{cases} i_{d\_\mathrm{mea}} = i_{d\_\mathrm{act}} + \Delta i_d \\ i_{q\_\mathrm{mea}} = i_{q\_\mathrm{act}} + \Delta i_q \end{cases} \tag{5}$$

where i_{x_mea} and $i_{x\_\mathrm{act}}, x = d$ and q are the measured and actual values of the dq-axis currents, and Δi_d and Δi_q are the errors between the measured and actual currents, respectively. Among (5), the error terms are

$$\begin{cases} \Delta i_d = \Delta i_a \cos\theta_e + \frac{1}{\sqrt{3}} (\Delta i_a + 2\Delta i_b) \sin\theta_e \\ \Delta i_q = -\Delta i_a \sin\theta_e + \frac{1}{\sqrt{3}} (\Delta i_a + 2\Delta i_b) \cos\theta_e \end{cases} \tag{6}$$

where θ_e represents the electrical angle, $\theta_e{=}\omega_e t{=}\ 2\pi f_e t$. Obviously, the error terms are related to the CMEs of phase a, b currents Δi_a, Δi_b and the stator electrical frequency f_e. Next, the dq-axis representations of offset error and scaling error are shown separately.

1) Offset Error: Considering offset error alone, the error terms of dq-axis currents are obtained by substituting $\Delta i_a{=}\Delta i_{a\_\mathrm{offset}}$, $\Delta i_b{=}\Delta i_{b\_\mathrm{offset}}$ into (6)

$$\begin{cases} \Delta i_d = I_1 \sin(\theta_e + \varphi_1) \\ \Delta i_q = I_1 \cos(\theta_e + \varphi_1) \end{cases} \tag{7}$$

where

$$\begin{cases} I_1 = \frac{2}{\sqrt{3}} \sqrt{(\Delta i_{a\_\mathrm{offset}})^2 + \Delta i_{a\_\mathrm{offset}} \Delta i_{b\_\mathrm{offset}} + (\Delta i_{b\_\mathrm{offset}})^2} \\ \varphi_1 = \tan^{-1}\left(\frac{\sqrt{3}\Delta i_{a\_\mathrm{offset}}}{\Delta i_{a\_\mathrm{offset}} + 2\Delta i_{b\_\mathrm{offset}}} \right). \end{cases}$$

Under the premise of correct execution of the control algorithm, the given and measured currents should be equal during the steady state, i.e., $i_q^* = i_{q\_\mathrm{mea}}$. Combining (2) and (10), the influence of offset error on electromagnetic torque is as follows:

$$T_e = k_T i_{q\_\mathrm{act}} = k_T \left(i_q^* - \Delta i_q \right) = T_e^* - \tau_1. \tag{8}$$

It can be seen from (8) that the disturbance torque τ_1 in the electromagnetic torque exists due to offset error. Through (7), further note that the electromagnetic torque will oscillate at the stator electrical frequency f_e.

2) Scaling Error: When referring to scaling error separately, it is generally assumed that the measured current remains sinusoidal

$$\begin{cases} i_{a\_\mathrm{mea}} = k_a i_{a\_\mathrm{act}} = I \cos(\theta_e + \phi) \\ i_{b\_\mathrm{mea}} = k_b i_{b\_\mathrm{act}} = I \cos\left(\theta_e - \frac{2}{3}\pi + \phi\right) \end{cases} \tag{9}$$

where $\phi = \tan^{-1}(i_{q\_\mathrm{mea}}/i_{d\_\mathrm{mea}})$ and I is the magnitude of the measured current. Combine (9) and (5), and further substitute into (8)

$$\begin{cases} \Delta i_d = I_2 \sin(2\theta_e + \varphi_2) + I_{2\_1} \\ \Delta i_q = I_2 \cos(2\theta_e + \varphi_2) + I_{2\_2} \end{cases} \tag{10}$$

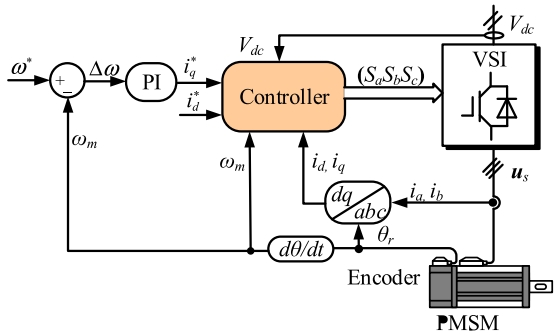

Fig. 1. Block diagram of motor control structure.

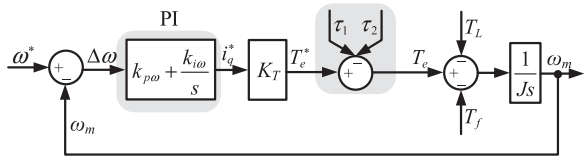

Fig. 2. Simplified speed loop block diagram.

where

$$\begin{cases} I_2 = \frac{I}{\sqrt{3}} \left(\frac{1}{k_a} - \frac{1}{k_b} \right) \\ \varphi_2 = \phi - \frac{2}{3}\pi \\ I_{2\_1} \\ \quad = \frac{I}{\sqrt{3}} \left\{ \left(1 - \frac{1}{k_b}\right) \sin\left(\frac{2}{3}\pi - \phi\right) + \left(1 - \frac{1}{k_a}\right) \sin\left(\frac{2}{3}\pi + \phi\right) \right\} \\ I_{2\_2} \\ \quad = \frac{I}{\sqrt{3}} \left\{ \left(1 - \frac{1}{k_b}\right) \cos\left(\frac{2}{3}\pi - \phi\right) - \left(1 - \frac{1}{k_a}\right) \cos\left(\frac{2}{3}\pi + \phi\right) \right\}. \end{cases}$$

Since I_{2_1} and I_{2_2} in (10) are constant, they are compensated by the speed controller during the steady state, so the remaining items are similar to the analysis of offset error. The disturbance torque τ_2 caused by the scaling error makes the electromagnetic torque oscillate at twice the stator frequency $2f_e$. Analyzing (7) and (10), it is obvious that the dq-axis CMEs is a sinusoidal signal, like$\Delta i_{x_\mathrm{error}} = I_{x_\mathrm{error}} \sin(\theta_{\mathrm{error}} + \varphi_{x_\mathrm{error}})$, $x = d, q$, error is offset error or scaling error. After being expanded, it is the sum of sinusoidal signals with coefficients.

C. Impacts of CMEs on Motor Performance

PMSM control usually adopts the double closed-loop control structure shown in Fig. 1. The outer loop is a common speed PI regulator, and the inner loop can be current or torque-flux control as required. This article mainly studies the traditional VC, so the controller includes two dq-axis current PI regulators, inverse Park transformation, and space voltage vector pulse width modulation (SVPWM).

If the motor drive system is well designed, the response of the inner loop control object is generally much shorter than the response of the mechanical system. Therefore, when analyzing the speed loop, the dynamic process of the inner loop can be ignored [27]. Then, simplify Fig. 1 and use Fig. 2 to represent it, where τ_1 and$\tau_2$are the pulsating torque caused by CMEs.

Derived from (3), the transfer function of the motor plant is

$$G_p(s) = \frac{k_T}{Js}$$
$$G_p(z) = G_p(s)\big|_{s=\frac{2}{T}\frac{z-1}{z+1}} = C_p\left(\frac{2}{T}\frac{z-1}{z+1}\right). \quad (11)$$

The input and output of (11) are the q-axis current and speed, respectively, which is applied to the subsequent ASHE algorithm. As shown in Fig. 2, the transfer function of the speed loop is

$$G_t(s) = \frac{k_T k_{p\omega} s + k_T k_{i\omega}}{Js^2 + k_T k_{p\omega} s + k_T k_{i\omega}}. \quad (12)$$

The speed loop can suppress the constant disturbance caused by the friction torque T_f and load torque T_L. In [28], pulsating torque in PMSM is usually generated by various sources, including cogging torque, flux harmonics, and current sensor errors. It is composed of the 1st, 2nd, 6th, and 12th harmonics with the fundamental is the synchronous frequency. The bandwidth of the load inertia and speed loop eliminates higher-order harmonics, but the middle and low frequency ripples within the bandwidth may still cause speed ripple. This article mainly focuses on the first and second harmonics caused by CMEs.

III. Improved ASHE Correction Strategy

Since CMEs cause the first and second harmonics of the motor speed. This article improves the ASHE algorithm that eliminates undesirable speed harmonics. The idea of the proposed method derives from the characteristics of CMEs, that is, the *dq*-axis current errors are sinusoidal signals. The classic ASHE algorithm eliminates the harmonics of the selected frequency from the target, and outputs the sum of sinusoidal signals with adaptive weights. The improved ASHE algorithm aims to suppress the speed ripple by separately compensating the *dq*-axis current.

A. Classical ASHE

The LMS adaptive algorithm is characterized by parallel computation, online adaptation, and simple implementation. The classical ASHE algorithm uses the LMS algorithm to update the weights online [24], and its structure is shown in Fig. 3. The reference signals $x_c(k)$and $x_s(k)$are sinusoidal references, k is the moment index, and T is the sampling period. In $x_c(k)$ and $x_s(k)$, the frequency $\omega_h = 2\pi f_h$ is the selected harmonic to be eliminated from primary input signal $d(k)$, $\varepsilon(k)$ is an error estimate, and $y(k)$ is the output signal. The error estimate $\varepsilon(k)$ is as follows:

$$\varepsilon(k) = d(k) - y(k)$$
$$= d(k) - \boldsymbol{X}^T(k)\boldsymbol{w}(k) \quad (13)$$

where $\boldsymbol{X}(k)$is the reference vector and $\boldsymbol{w}(k)$is weight vector, they are defined as

$$\boldsymbol{X}^T(k) = \left[x_c(k)\ x_s(k)\right] = \left[\cos\omega_h kT\ sin\omega_h kT\right]$$
$$\boldsymbol{w}^T(k) = \left[w_c(k)\ w_s(k)\right]. \quad (14)$$

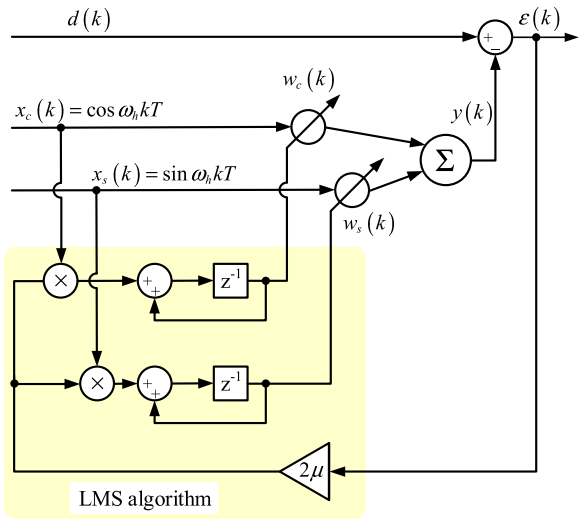

Fig. 3. Structure of the classical ASHE algorithm.

The multiplication of the above two vectors can be used to match the amplitude and phase of the sinusoidal interference in the primary input signal. With the LMS algorithm, the adaptive update of weights can be expressed as

$$\boldsymbol{w}(k+1) = \boldsymbol{w}(k) + 2\mu \cdot \boldsymbol{X}(k) \cdot \varepsilon(k) \quad (15)$$

where μ is the adaptation gain constant, it regulates the convergence speed and algorithm stability. By analyzing the signal propagation in Fig. 3, the mechanism of the classical ASHE algorithm is illustrated [26]. The transfer function $G(z)$ from $\varepsilon(k)$ to $y(k)$ in the z-domain is

$$G(z) = \frac{2\mu(z\cos\omega_h T - 1)}{z^2 - 2z\cos\omega_h T + 1}. \quad (16)$$

B. Adopting Classical ASHE for q-Axis Current Compensation

In this article, the purpose is to suppress speed ripple caused by CMEs, and the ASHE algorithm is adopted. When the ASHE algorithm is applied, the plant should be considered. Thus, the output $y(k)$ is multiplied with the inverse transfer function $G_p^{-1}(z)$ of the plant. In detail, the input $d(k)$ is the speed tracking error, the selected frequency ω_h is the stator electrical frequency corresponding to the speed reference, and the q-axis current compensation i_{q_ASHE} is the output. The structure diagram is shown in Fig. 4, including the motor speed control system model and the ASHE algorithm with $G_p^{-1}(z)$. $\bar{\omega}$ is the speed error without the influence of CMEs, and ε_ω is the speed error after the influence of the q-axis CMEs Δi_q, including $\bar{\omega}$ and speed harmonics $\Delta\omega$, $\tilde{\omega}$ are the compensated speed corresponding to i_{q_ASHE}, and $\widehat{\omega}$ is the speed error after compensation. The principle is that after compensation, the speed error ε_ω should be significantly reduced. $G_p^{-1}(z)$is obtained from (11)

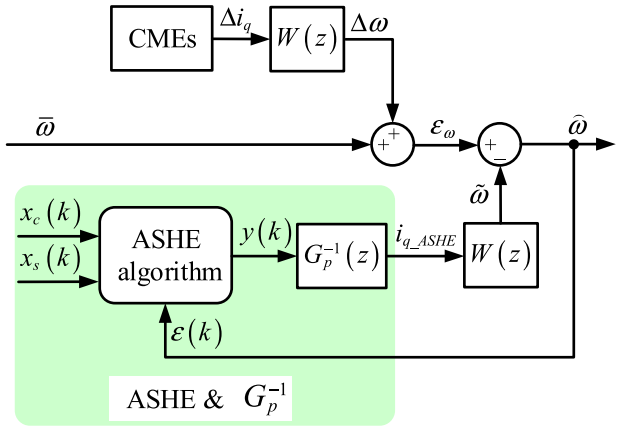

Fig. 4. Current compensation based on the ASHE algorithm.

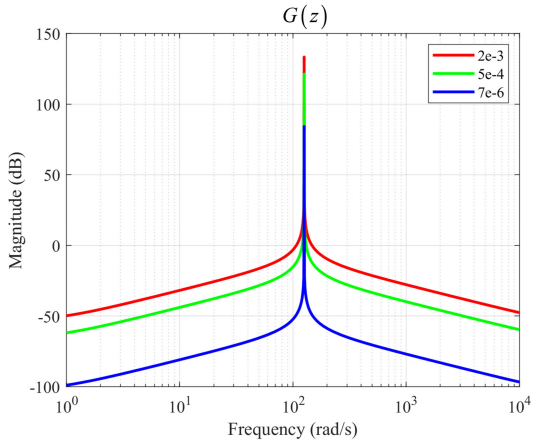

Fig. 5. Frequency response of $G(z)$ with different μ.

$$G_p^{-1}(s) = \frac{Js}{k_T}$$

$$G_p^{-1}(z) = G_p^{-1}(s)\big|_{s=\frac{2}{T}\frac{z-1}{z+1}} = G_p^{-1}\left(\frac{2}{T}\frac{z-1}{z+1}\right). \quad (17)$$

In addition, $W(z)$ is the transfer function, which represents the dynamic response of the q-axis current to the speed. $W(z)$ is expressed as

$$W(s) = \frac{\Delta\omega(s)}{\Delta i_q(s)} = \frac{\tilde{\omega}(s)}{i_{q\_\mathrm{ASHE}}(s)} = \frac{k_T s}{Js^2 + k_T k_{p\omega} s + k_T k_{i\omega}}$$

$$W(z) = W(s)|_{s=\frac{2}{T}\frac{z-1}{z+1}} = W\left(\frac{2}{T}\frac{z-1}{z+1}\right). \quad (18)$$

The transfer function $G(z)$ of the ASHE algorithm can better illustrate the extraction of harmonic components. Fig. 5 shows the frequency response curve of $G(z)$ with different step size μ. The selected frequency ω_h is 40π rad/s. If 40π rad/s is the second harmonic, the corresponding motor fundamental electrical frequency should be 10 Hz, and the mechanical speed should be 150 r/min. Through $G(z)$, the frequency ω_h part of the error $\varepsilon(k)$ is significantly increased, and the gain degree is positively related to the step size.

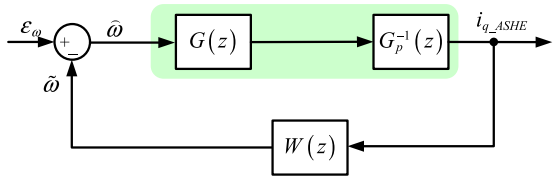

Fig. 6. Block diagram of the ASHE algorithm applied to current compensation.

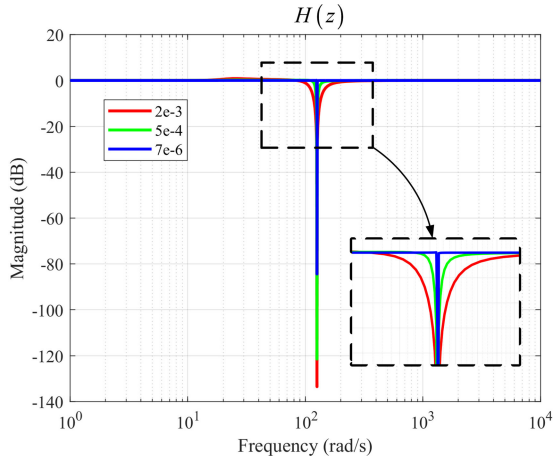

Fig. 7. Frequency response of $H(z)$ with different μ.

In order to analyze the ASHE algorithm's influence on the speed error, the block diagram from the speed error ε_ω to the q-axis current compensation is shown in Fig. 6. The transfer function $H(z)$ from ε_ω to $\widehat{\omega}$ in the z-domain is

$$H(z) = \frac{1}{1 + W(z)\,G(z)\,G_p^{-1}(z)}. \quad (19)$$

The frequency response of $H(z)$ with different step size μ is shown in Fig. 7. It can be seen that the ASHE algorithm actually realizes the function of a notch filter. Fig. 7 shows that the gain of the target frequency is greatly reduced with a narrow notch. On the other hand, at other frequencies, the gain keeps 0 dB. This means that the proposed method can greatly mitigate the second harmonic component of the speed without affecting other frequency components. As step size μ increases, the notch range becomes wider and the attenuation is aggravated accordingly. Conversely, reducing step size μ will result in unsatisfactory notch effects and slow convergence. Therefore, the step size μ can neither be too large nor too small, and an appropriate value should be selected.

Using the ASHE algorithm alters the dynamic response of the q-axis current to the speed. The block diagram is shown in Fig. 8, where $G_\omega(z)$ is the speed PI controller

$$C_\omega(s) = \frac{k_{p\omega} s + k_{i\omega}}{s}$$

$$C_\omega(z) = C_\omega(s)|_{s=\frac{2}{T}\frac{z-1}{z+1}} = C_\omega\left(\frac{2}{T}\frac{z-1}{z+1}\right). \quad (20)$$

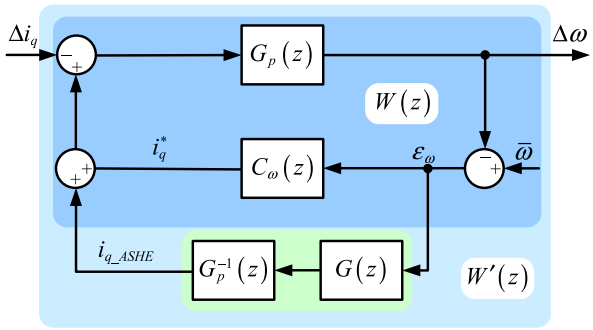

Fig. 8. Equivalent block diagram with q-axis current error after compensation.

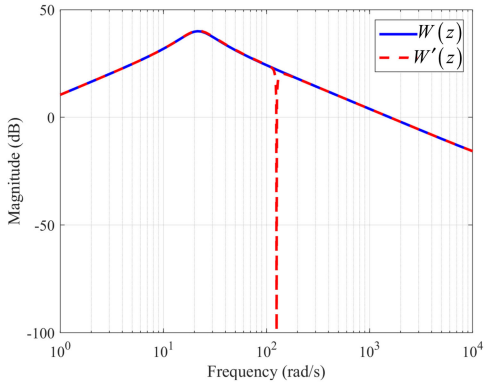

Fig. 9. Frequency response of $W(z)$ and $W'(z)$.

The new transfer function $W'(z)$ is written as

$$W'(z)=\frac{G_p(z)}{1+G_p(z)\left(C_\omega(z)+G(z)G_p^{-1}(z)\right)}. \tag{21}$$

Fig. 9 shows the frequency responses of the transfer functions $W(z)$ and $W'(z)$ before and after compensation. The sole difference is that the selected frequency of $W'(z)$ is significantly attenuated. Through the speed error, the applied ASHE algorithm outputs the q-axis current compensation for the motor CMEs.

Assuming that the slowly changing weights $w_c(k)$ and $w_s(k)$ are constant, the q-axis current compensation at instant k is

$$\begin{aligned} i_{q\_\mathrm{ASHE}} &= G_p^{-1}(s)\,y(k) \\ &= G_p^{-1}(s)\left(\boldsymbol{X}^T(k)\,\boldsymbol{w}(k)\right) \\ &= G_p^{-1}(s)\left(w_c(k)\,x_c(k)+w_s(k)\,x_s(k)\right). \end{aligned} \tag{22}$$

Combining (14) and (17), (22) can be converted to

$$\begin{aligned} i_{q\_\mathrm{ASHE}} &= \frac{J}{k_T}s\left(w_c(k)\cos\omega_h kT+w_s(k)\,sin\omega_h kT\right) \\ &= \omega_h\frac{J}{k_T}\left(-w_c(k)\sin\omega_h kT+w_s(k)\cos\omega_h kT\right). \end{aligned} \tag{23}$$

For other constant items of reference signals' coefficients, because the LMS algorithm updates the weights adaptively online, they can be ignored. The outputs of the LMS algorithm

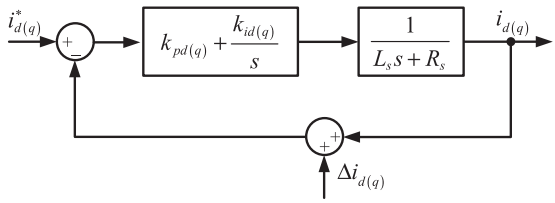

Fig. 10. dq-axis current block diagram.

is weight vector $(\boldsymbol{w}^*)^T=[\,w_c^*(k)\;w_s^*(k)\,]$ combined with the constant terms, so (23) is rewritten as

$$i_{q\_\mathrm{ASHE}}=w_s^*(k)\cos\omega_h kT-w_c^*(k)\sin\omega_h kT \tag{24}$$

where

$$\begin{cases} w_c^*(k)=\omega_h\frac{J}{k_T}w_c(k) \\ w_s^*(k)=\omega_h\frac{J}{k_T}w_s(k). \end{cases}$$

Although the weights' signs change, the calculation process of the weight adaptation is still the same as (15)

$$\boldsymbol{w}^*(k+1)=\boldsymbol{w}^*(k)+2\mu\cdot\boldsymbol{X}(k)\cdot\varepsilon(k). \tag{25}$$

C. Improving ASHE for d-Axis Current Compensation

Through the deterministic function (17), the implemented ASHE algorithm outputs the q-axis current compensation (24). However, even if the q-axis current compensation reduces the speed ripple, it fails to thoroughly suppress the negative effects of CMEs. In the traditional VC method, when the back EMF is ignored, the current loop model is shown in Fig. 10. The transfer function of the current loop is described as

$$C_{d(q)}(s)=\frac{k_{pd(q)}s+k_{id(q)}}{L_s s^2+\left(R_s+k_{pd(q)}\right)s+k_{id(q)}}. \tag{26}$$

Since (26) is a second-order transfer function, the dq-axis current harmonics generated by CMEs cannot be eliminated by current closed loop alone. The applied ASHE algorithm compensates the q-axis CMEs and reduces speed ripple, but does not eliminate the d-axis CMEs, which will lead to poor current performance, whereas, it is remarkable that there is uncertainty in the relationship between d-axis current and speed. Therefore, the ASHE algorithm needs to be improved to simultaneously compensate the dq-axis CMEs.

Then, taking the fundamental frequency f_e as an example, that is $\omega_h{=}\omega_e$, (7) can be expanded as

$$\begin{cases} \Delta i_d=I_1\sin(\omega_h kT+\varphi_1) \\ \quad =I_1\sin\varphi_1\cos\omega_h kT+I_1\cos\varphi_1\sin\omega_h kT \\ \Delta i_q=I_1\cos(\omega_h kT+\varphi_1) \\ \quad =I_1\cos\varphi_1\cos\omega_h kT-I_1\sin\varphi_1\sin\omega_h kT. \end{cases} \tag{27}$$

Obviously, the q-axis current compensation output and the dq-axis CMEs are all the weighted sums of sinusoidal signals, so the ASHE weights can also be used to obtain d-axis current compensation. Further improve the ASHE algorithm, combining (24) and (27), the corresponding relationship between the

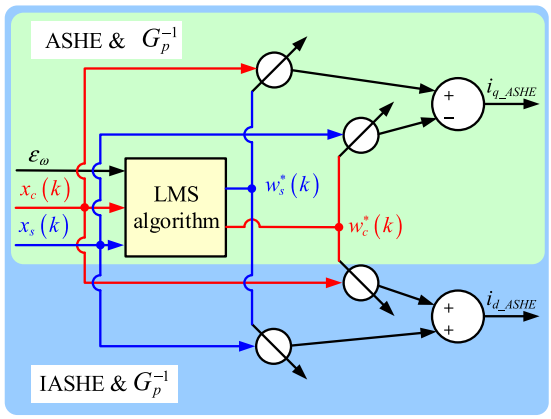

Fig. 11. Block diagram of the IASHE algorithm.

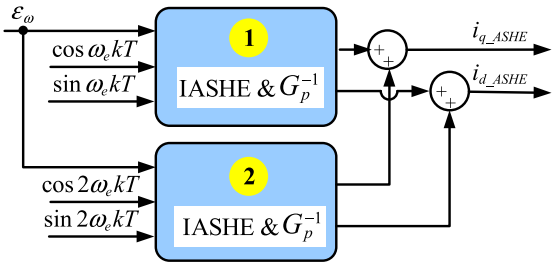

Fig. 12. Block diagram of the IASHE algorithm for the motor CMEs problem.

weights is as follows:

$$\begin{cases} I_1 \sin\varphi_1 = w_c^*(k) \\ I_1 cos\varphi_1 = w_s^*(k). \end{cases} \tag{28}$$

Thus, the d-axis current compensation is obtained

$$i_{d\_\mathrm{ASHE}} = w_c^*(k)\cos\omega_h kT + w_s^*(k)\sin\omega_h kT. \tag{29}$$

Using (24), (25), and (29), the proposed method compensates the dq-axis CMEs simultaneously and respectively.

D. Implementation of Improved ASHE on VC

Combined with the improved ASHE (IASHE) algorithm, Fig. 11 shows the block diagram of IASHE algorithm. The inputs are the speed error ε_ω and the reference vector $\boldsymbol{X}(k)$, and the outputs are the dq-axis current compensation i_{d_ASHE} and i_{q_ASHE}. The complexity of the calculation process does not increase. Besides, none of the motor parameters are required.

For other harmonics, such as double fundamental frequency, a second block can be added to the first block of the fundamental frequency to expand and eliminate harmonic components. The IASHE algorithm for the motor CMEs problem is shown in Fig. 12. The added block only changes frequency of the reference signals, and the outputs are summed up accordingly. Furthermore, similar blocks can also be used for other higher-order harmonics.

In terms of traditional VC method, the controller includes two PI regulators, inverse Park transform and SVPWM. Fig. 13 illustrates the implementation of the IASHE algorithm on VC

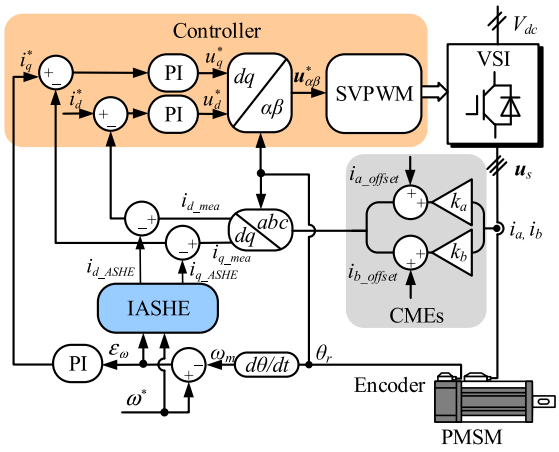

Fig. 13. Implementation of IASHE algorithm on VC method of PMSMs.

TABLE I
SYSTEM PARAMETERS

TABLE I
SYSTEM PARAMETERS

Symbol	Parameter	Value
P_N	Rated power	0.4 *kW*
R_s	Resistance	2.35 *Ω*
L_d / L_q	*d*-/*q*-axis inductance	6.5 *mH*
ψ_{PM}	PM flux linkage	0.07876 *V·s*
p	Number of pole pairs	4
n_N	Rated speed	3000 *r/min*
J	The moment of inertia	0.0003 *kgm²*
T_N	Rated torque	1.27 *Nm*
i_N	Rated current	2.8 *A*
k_a	Phase *a* scaling error	1.01
Δi_{a_offset}	Phase *a* offset error	0.15 *A*
k_b	Phase *b* scaling error	0.98
Δi_{b_offset}	Phase *b* offset error	-0.1 *A*

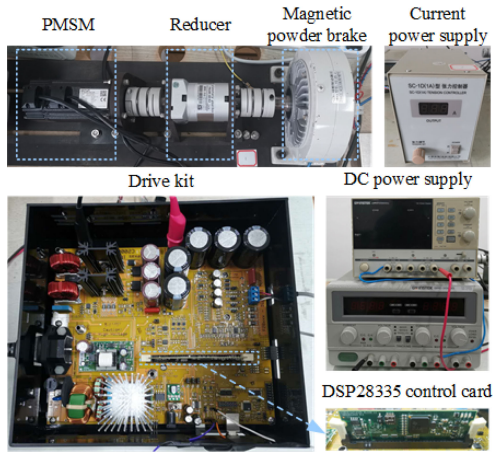

Fig. 14. Experimental platform.

method. The algorithm is designed to compensate the dq-axis synchronous currents. Obviously, the proposed method does not change the traditional control structure. Therefore, the modifications to other modern control technologies are the same as that of VC.

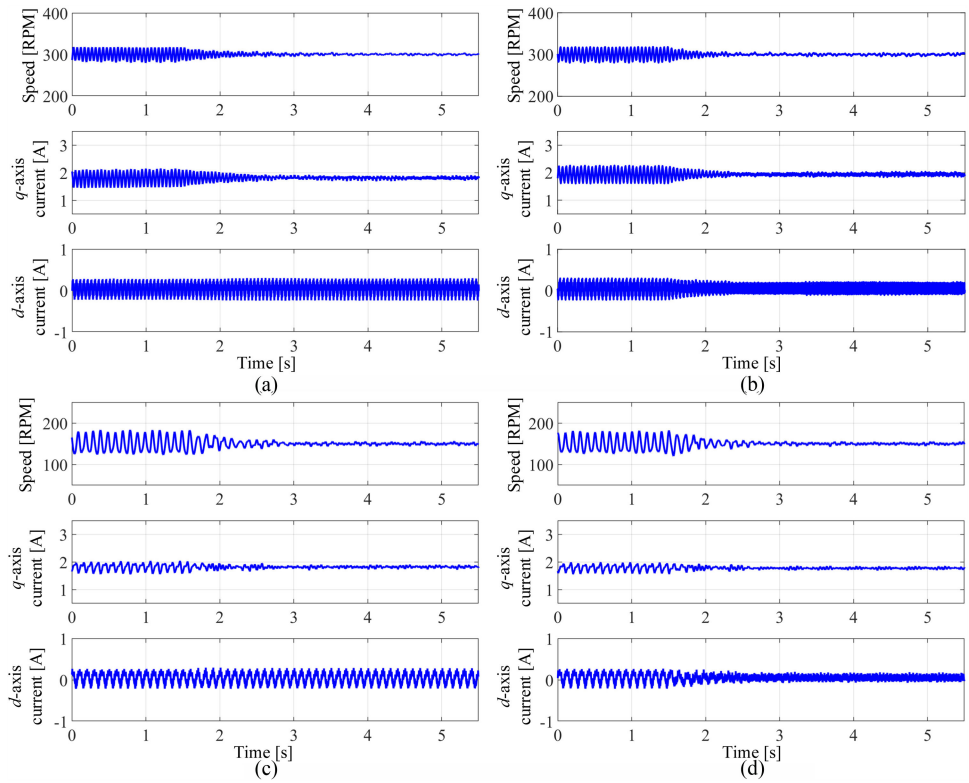

Fig. 15. Waveforms before and after compensation: (from top to bottom) speed, q-axis current, and d-axis current. (a) 300 r/min, ASHE algorithm. (b) 300 r/min, IASHE algorithm. (c) 150 r/min, ASHE algorithm. (d) 150 r/min, IASHE algorithm.

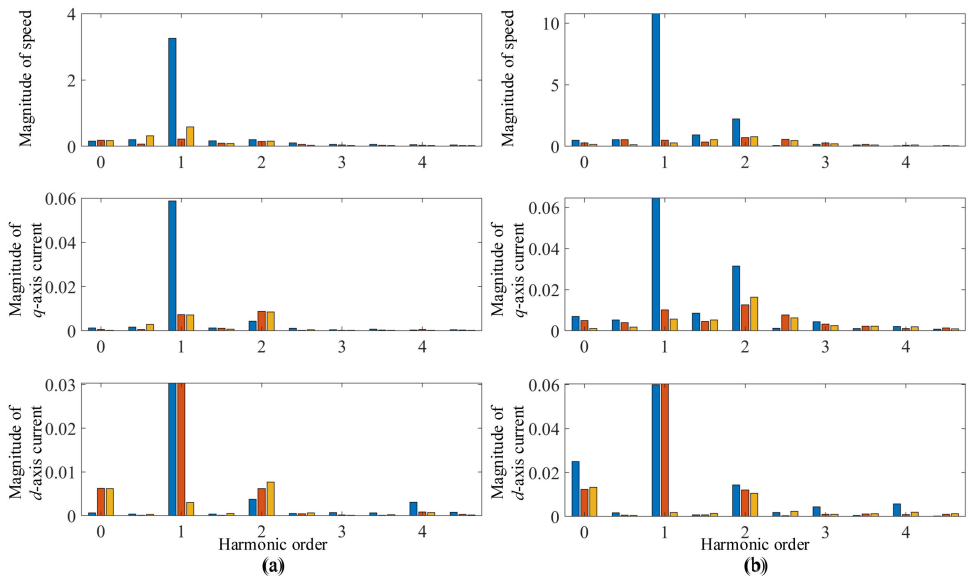

Fig. 16. FFT analysis of speed error, q-axis, and d-axis currents, (blue, red, and orange are without compensation, compensation by ASHE algorithm, and IASHE algorithm). (a) 300 r/min. (b) 150 r/min.

In the proposed method, the key parameter is the step size μ of the LMS algorithm, which is related to the stability of the system and the speed of convergence. Regarding system stability, μ does not allow arbitrary settings. Generally, the larger μ may increase the convergence speed, but also easily triggers instability. On the other hand, if the step size μ is small, the convergence speed will be slow, resulting in unsatisfactory performance. Therefore, the step size μ should be appropriate, neither too large nor too small. When debugging, a smaller value can be gradually increased to achieve a satisfactory result. This article mainly

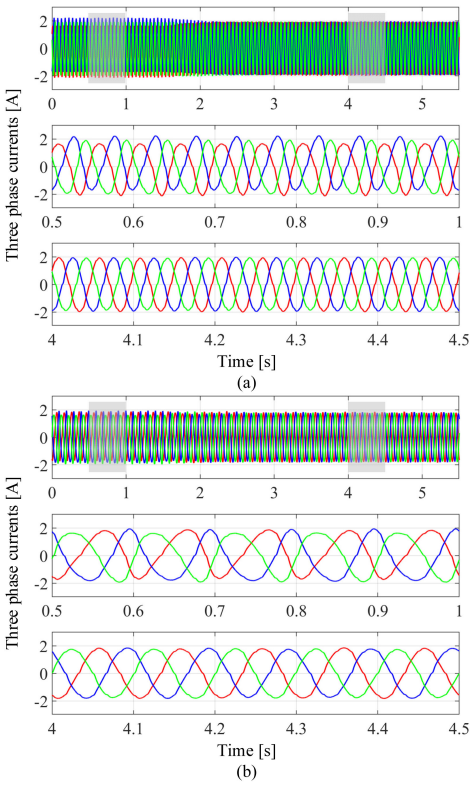

Fig. 17. Three phase currents. (a) 300 r/min. (b) 150 r/min.

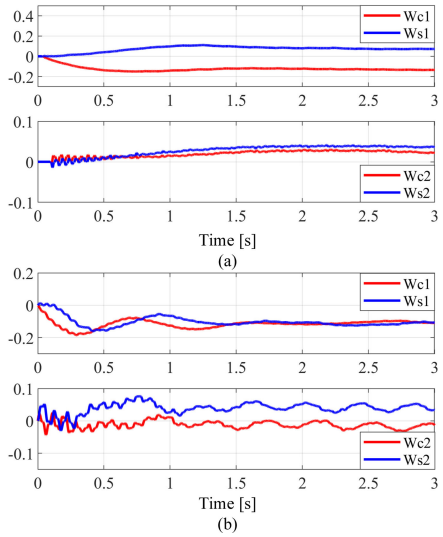

Fig. 18. Weights of IASHE algorithm. (a) 300 r/min. (b) 150 r/min.

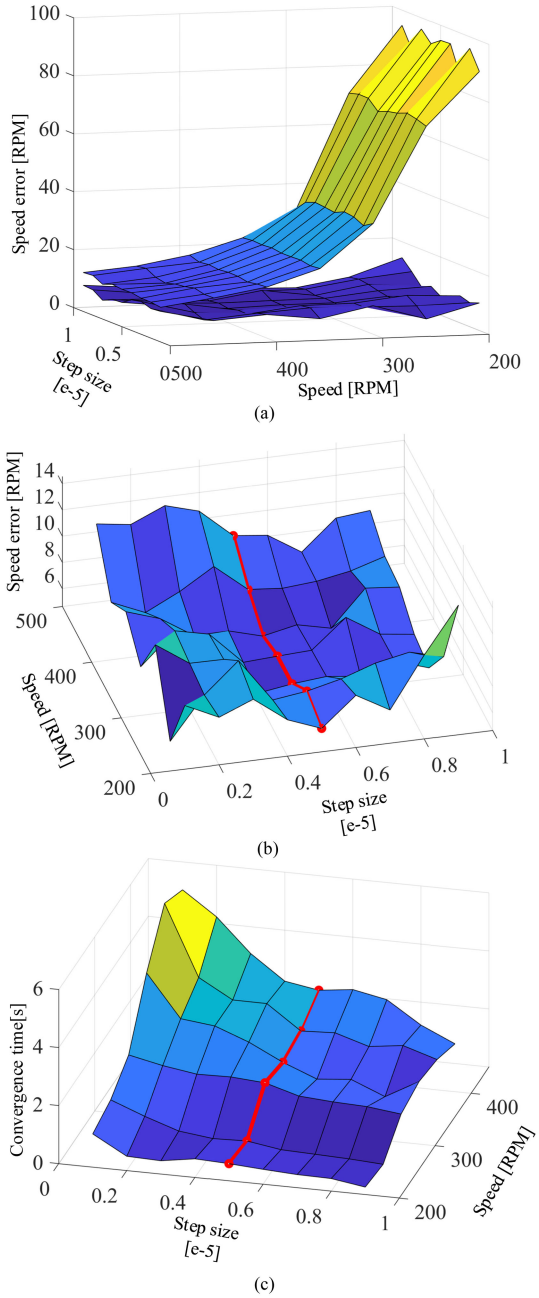

Fig. 19. Experimental results of different step sizes and speeds. (a) Peak-to-peak value measurement comparison of speed ripple error before and after compensation. (b) Peak-to-peak value of speed ripple error after compensation. (c) Convergence time required for stabilization.

tests the effectiveness of the proposed method, so the standard LMS algorithm is adopted with $\mu = 5\text{e} - 6$.

IV. Experimental Results

The application of the proposed method in VC has been tested in a SPMSM 2L-VSI drive platform. The system parameters are shown in Table I, and Fig. 14 is the photograph of the equipment. The load side machine is an FZ 25. *J* magnetic powder brake, which is driven by an SC-1D tension controller. This article uses the DSP-F28335 embedded platform to implement algorithms, and the control period is 62.5 μs, that is, the interrupt frequency is 16 kHz. The currents are sampled through 12-bit ADCs, and the integrated low side resistive shunts are used to measure the currents.

Fig. 15 shows the waveforms before and after compensation using the ASHE and proposed IASHE algorithms with reference speeds of 300 and 150 r/min. Before compensation, CMEs cause

dq-axis current and speed ripples. As the speed increases, the stator electrical frequency and speed harmonic frequency become higher. After the ASHE algorithm performs compensation, the speed and *q*-axis current ripples are suppressed. However, the *d*-axis current still has obvious ripple, which indicates that the *d*-axis CMEs are not eliminated. Using the IASHE algorithm, the *d*-axis current ripple is also suppressed. The proposed IASHE algorithm compensates *dq*-axis CMEs and suppresses speed ripple.

Fig. 16 shows the FFT results before and after compensation using the ASHE and proposed IASHE algorithms. When the speed references are 300 and 150 r/min, the stator electrical frequencies are 20 and 10 Hz, respectively. When the speed is 300 r/min, Fig. 16(a) shows that the ripples mainly concentrate on the fundamental frequency. In Fig. 16(b), the speed is 150 r/min and the double fundamental harmonic increases. The reason for this phenomenon is consistent with the analysis in Section II-C: due to the existence of the speed PI regulator and the moment of inertia bandwidth, even if scaling error exists, no higher order harmonics like double fundamental frequency are observed. Compared with the ASHE algorithm, the improved algorithm not only attenuates the harmonics of speed and *q*-axis current, but also *d*-axis current.

The three phase current waveforms before and after compensation by IASHE algorithm are shown in Fig. 17. After compensation, the distorted three phase currents are restored to balance. It shows that the simultaneous compensation of the *dq*-axis current is to correct CMEs. The method proposed in this article suppresses the negative effects of CMEs.

The phenomenon of weights in Fig. 18 also reflects the working mechanism of the proposed method. Wc1 and Ws1 are the weights of the first block, and Wc2 and Ws2 represent the weights of the second block. After starting the compensation, the weights change until reaching a stable mutual equilibrium state. These adaptive weights are linearly combined with sinusoidal signals of known electrical frequency to counteract the *dq*-axis CMEs.

Fig. 19 shows the experimental results of different speeds and step sizes. In Fig. 19(a), as the speed increases, the speed ripple decreases. It is consistent with the above analysis. Due to the bandwidth of the speed PI regulator and the moment of inertia, the higher harmonics of the speed are suppressed. After the compensation of the proposed method, the speed error is significantly reduced. The compensation effect and time of reaching steady state are shown in Fig. 19(b) and (c). As step size increases, the convergence speed increases, and the time for stabilization decreases, but the error reduction effect is not good. Conversely, when step size reduces, the notch effect is not ideal, and the convergence time is greatly increased. Therefore, considering the overall performance, the step size in this article is $5e-6$, which is the red line part of Fig. 19(b) and (c).

V. Conclusion

The problem of CMEs in the motor produces speed and torque ripples with one and twice the stator electrical frequency. This article proposes a CME correction method for PMSMs. The improved ASHE algorithm is used to directly estimate and compensate the *dq*-axis CMEs. In terms of performance, speed ripple is suppressed, the three phase currents are restored to balance, and the negative effects of CMEs are suppressed.

The main contributions of this article are that the ASHE algorithm is adopted to solve the CME problem, and compensates *q*-axis current with the deterministic functional relationship between speed and *q*-axis current. In addition, for no explicit connection between speed and *d*-axis current, this article uses the mutual deterministic connection of *dq*-axis CMEs to obtain the *d*-axis current compensation.

The proposed method does not require additional sensor, motor parameter, and complex calculation process. Besides, it does not change the structure of modern motor control technologies and has wide applicability. Except for the common VC, the proposed method is suitable for other technologies, such as direct torque control and model predictive control. The higher-order harmonics can also be the targets for the improved ASHE algorithm.

References

[1] Y. Yang *et al.*, "Design and comparison of interior permanent magnet motor topologies for traction applications," *IEEE Trans. Transp. Electrif.,* vol. 3, no. 1, pp. 86–97, Mar. 2017.

[2] S. Li, B. Sarlioglu, S. Jurkovic, N. R. Patel, and P. Savagian, "Comparative analysis of torque compensation control algorithms of interior permanent magnet machines for automotive applications considering the effects of temperature variation," *IEEE Trans. Transp. Electrif.,* vol. 3, no. 3, pp. 668–681, Sep. 2017.

[3] Z. Yang, F. Shang, I. P. Brown, and M. Krishnamurthy, "Comparative study of interior permanent magnet, induction, and switched reluctance motor drives for EV and HEV applications," *IEEE Trans. Transp. Electrif.,* vol. 1, no. 3, pp. 245–254, Oct. 2015.

[4] S. Choi *et al.*, "Fault diagnosis techniques for permanent magnet AC machine and Drives—A review of current state of the art," *IEEE Trans. Transp. Electrif.,* vol. 4, no. 2, pp. 444–463, Jun. 2018.

[5] H. A. Young, M. A. Perez, J. Rodriguez, and H. Abu-Rub, "Assessing finite-control-set model predictive control: A comparison with a linear current controller in two-level voltage source inverters," *IEEE Ind. Electron. Mag.,* vol. 8, no. 1, pp. 44–52, Mar. 2014.

[6] J. Holtz, "Advanced PWM and predictive control—An overview," *IEEE Trans. Ind. Electron.,* vol. 63, no. 6, pp. 3837–3844, Jun. 2016.

[7] J. Holtz and Q. Juntao, "Drift- and parameter-compensated flux estimator for persistent zero-stator-frequency operation of sensorless-controlled induction motors," *IEEE Trans. Ind. Appl.,* vol. 39, no. 4, pp. 1052–1060, Jul./Aug. 2003.

[8] J. Lu, Y. Hu, G. Chen, Z. Wang, and J. Liu, "Mutual calibration of multiple current sensors with accuracy uncertainties in IPMSM drives for electric vehicles," *IEEE Trans. Ind. Electron.,* vol. 67, no. 1, pp. 69–79, Jan. 2020.

[9] S. K. Kommuri, S. B. Lee, and K. C. Veluvolu, "Robust sensors-fault-tolerance with sliding mode estimation and control for PMSM drives," *IEEE-ASME Trans. Mechatron.,* vol. 23, no. 1, pp. 17–28, Feb. 2018.

[10] Q. N. Trinh, P. Wang, Y. Tang, L. H. Koh, and F. H. Choo, "Compensation of DC offset and scaling errors in voltage and current measurements of three-phase AC/DC converters," *IEEE Trans. Power Electron.,* vol. 33, no. 6, pp. 5401–5414, Jun. 2018.

[11] W. Qian, S. K. Panda, and J.-X. Xu, "Torque ripple minimization in PM synchronous motors using iterative learning control," *IEEE Trans. Power Electron.,* vol. 19, no. 2, pp. 272–279, Mar. 2004.

[12] M. Hu, W. Hua, Z. Wu, N. Dai, H. Xiao, and W. Wang, "Compensation of current measurement offset error for permanent magnet synchronous machines," *IEEE Trans. Power Electron.,* vol. 35, no. 10, pp. 11119–11128, Oct. 2020.

[13] C. Dae-Woong and S. Seung-Ki, "Analysis and compensation of current measurement error in vector-controlled AC motor drives," *IEEE Trans. Ind. Appl.,* vol. 34, no. 2, pp. 340–345, Mar./Apr. 1998.

[14] J. Richter and M. Doppelbauer, "Control and mitigation of current harmonics in inverter-fed permanent magnet synchronous machines with non-linear magnetics," *IET Power Electron.,* vol. 9, no. 10, pp. 2019–2026, Apr. 2016.
[15] Y. Yan, J. Yang, Z. Sun, C. Zhang, S. Li, and H. Yu, "Robust speed regulation for PMSM servo system with multiple sources of disturbances via an augmented disturbance observer," *IEEE-ASME Trans. Mechatron.,* vol. 23, no. 2, pp. 769–780, Apr. 2018.
[16] K. R. Cho and J. K. Seok, "Correction on current measurement errors for accurate flux estimation of AC drives at low stator frequency," *IEEE Trans. Ind. Appl.,* vol. 44, no. 2, pp. 594–603, Mar./Apr. 2008.
[17] H. S. Jung, S. H. Hwang, J. M. Kim, C. U. Kim, and C. Choi, "Diminution of current-measurement error for vector-controlled ac motor drives," *IEEE Trans. Ind. Appl.,* vol. 42, no. 5, pp. 1249–1256, Sep./Oct. 2006.
[18] M. C. Harke, J. M. Guerrero, M. W. Degner, F. Briz, and R. D. Lorenz, "Current measurement gain tuning using high-frequency signal injection," *IEEE Trans. Ind. Appl.,* vol. 44, no. 5, pp. 1578–1586, Sep./Oct. 2008.
[19] M. C. Harke and R. D. Lorenz, "The spatial effect and compensation of current sensor differential gains for three-phase three-wire systems," *IEEE Trans. Ind. Appl.,* vol. 44, no. 4, pp. 1181–1189, Jul./Aug. 2008.
[20] B. Widrow and D. Stearns, *Adaptive Signal Processing*. Englewood Cliffs, NJ, USA: Prentice-Hall, 1985.
[21] V. Blasko, "A novel method for selective harmonic elimination in power electronic equipment," *IEEE Trans. Power Electron.,* vol. 22, no. 1, pp. 223–228, Jan. 2007.
[22] V. Blasko, L. Arnedo, P. Kshirsagar, and S. Dwari, "Control and elimination of sinusoidal harmonics in power electronics equipment: A system approach," in *Proc. IEEE Energy Convers. Congr. Expo.*, Sep. 2011, pp. 2827–2837.
[23] R. R. Pereira, C. H. da Silva, L. E. B. da Silva, G. Lambert-Torres, and J. O. P. Pinto, "New strategies for application of adaptive filters in active power filters," *IEEE Trans. Ind. Appl.,* vol. 47, no. 3, pp. 1136–1141, May/Jun. 2011.
[24] J. Hong and R. Cao, "Adaptive selective harmonic elimination model predictive control for three-level T-Type inverter," *IEEE Access,* vol. 8, pp. 157983–157994, Aug. 2020.
[25] G. Zhang, G. Wang, D. Xu, and N. Zhao, "ADALINE-network-based PLL for position sensorless interior permanent magnet synchronous motor drives," *IEEE Trans. Power Electron.,* vol. 31, no. 2, pp. 1450–1460, Feb. 2016.
[26] Z. Tang and B. Akin, "A new LMS algorithm based deadtime compensation method for PMSM FOC drives," *IEEE Trans. Ind. Appl.,* vol. 54, no. 6, pp. 6472–6484, Nov./Dec. 2018.
[27] N. Liu, C. Xia, Z. Zhou, Y. Yan, and T. Shi, "Smooth speed control for permanent magnet synchronous motor using proportional gain compensation," *Diangong Jishu Xuebao/Trans. China Electrotechnical Soc.,* vol. 33, no. 17, pp. 4007–4015, 2018.
[28] J. Yang, W.-H. Chen, S. Li, L. Guo, and Y. Yan, "Disturbance /uncertainty estimation and attenuation techniques in PMSM Drives—A survey," *IEEE Trans. Ind. Electron.,* vol. 64, no. 4, pp. 3273–3285, Apr. 2017.

Kai Zhang (Graduate Student Member, IEEE) received the B.S. degree in engineering in 2019 from Soochow University, Suzhou, China, where he is currently working toward the M.S. degree in engineering with the School of Rail Transportation.

His research interest includes model predictive control for electric drives.

Mingdi Fan (Senior Member, IEEE) received the B.S. degree in electrical engineering and the Ph.D. degree in detection technology and automation device from Northwestern Polytechnical University, Xi'an, China, in 2008 and 2014, respectively.

From 2010 to 2011, he was a Visiting Scholar with the University of Kassel, Kassel, Germany. He is currently an Associate Professor with the School of Rail Transportation, Soochow University, Suzhou, China. His current research interests include model predictive control for power converters and motor drives.

Yong Yang (Senior Member, IEEE) received the B.S. degree in automation from Xiangtan University, Xiangtan, China, in 2003, the M.S. degree in electrical engineering from Guizhou University, Guiyang, China, in 2006, and the Ph.D. degree in electrical engineering from Shanghai University, Shanghai, China, in 2010.

From 2017 to 2018, he was a Visiting Scholar with the Center for High Performance Power Electronics (CHPPE), The Ohio State University, Columbus, OH, USA. He is currently an Associate Professor with the School of Rail Transportation, Soochow University, Suzhou, China. He has coauthored more than 60 journal articles and conference papers. His current research interests include model predictive control in power electronic converters, distributed energy resource interfacing, and high-performance motor drive control.

Zhongkui Zhu received the B.S and M.S. degrees in vehicle engineering from Hefei University of Technology, Hefei, China, in 1997 and 2002, respectively, and the Ph.D degree in instrumentation science and technology from the University of Science and Technology of China, Hefei, China, in 2002.

From 2005 to 2012, he was a Lecturer and an Associate Professor with the School of Mechanical and Electrical Engineering, Soochow University, Suzhou, China. Since 2012, he has been a Professor with the School of Rail Transportation, Soochow University. He is the author of more than 100 articles. His research interests include system monitoring and diagnostics, signal processing, and vehicle system dynamics and control.

Cristian Garcia (Member, IEEE) received the M.Sc. and Ph.D. degrees in electronics engineering from the Universidad Tecnica Federico Santa Maria (UTFSM), Valparaiso, Chile, in 2013 and 2017, respectively.

In 2016, he was a Visiting Ph.D. Student with the Power Electronics Machines and Control (PEMC) Group, University of Nottingham, Nottingham, U.K. From 2017 to 2019, he was an Assistant Professor with the Engineering Faculty, Universidad Andres Bello, Santiago, Chile. Since 2019, he has been with the Department of Electrical Engineering, University of Talca, Curico, Chile, where he is currently an Assistant Professor. His research interests include electric transportation applications, variable-speed drives, and model predictive control of power converters and drives.

Jose Rodriguez (Life Fellow, IEEE) received the Engineering degree in electrical engineering from the Universidad Tecnica Federico Santa Maria, Valparaiso, Chile, in 1977, and the Dr.-Ing. degree in electrical engineering from the University of Erlangen, Erlangen, Germany, in 1985.

Since 1977, he has been with the Department of Electronics Engineering, Universidad Tecnica Federico Santa Maria, where he was a Full Professor and the President. Since 2015, he has been the President, and since 2019, he has been a Full Professor with Universidad Andres Bello, Santiago, Chile. He has coauthored two books, several book chapters, and more than 400 journal and conference papers. His main research interests include multilevel inverters, new converter topologies, control of power converters, and adjustable-speed drives.

Dr. Rodriguez is a member of the Chilean Academy of Engineering. He was the recipient of a number of best paper awards from journals of the IEEE. In 2014, he was the recipient of the National Award of Applied Sciences and Technology from the Government of Chile. In 2015, he was the recipient of the Eugene Mittelmann Award from the Industrial Electronics Society of the IEEE. From 2014 to 2019, he has been included in the list of Highly Cited Researchers published by Web of Science.